Semiconductor Physics, Quantum Electronics & Optoelectronics, 2023. V. 26, No 3. P. 270-277.

Semiconductor physics

Preparation and ionic conductivity of Ag_8GeS_6-based ceramic materials

A.I. Pogodin[1*], M.J. Filep[1,2], S. Vorobiov[3], V. Komanicky[3], T.O. Malakhovska[1], O.P. Kokhan[1], V.V. Vakulchak[1]

[1]*Uzhhorod National University, 46, Pidgirna str., 88000 Uzhhorod, Ukraine*
[2]*Ferenc Rákóczi II Transcarpathian Hungarian Institute, Kossuth Sq. 6, Beregovo 90200, Ukraine*
[3]*P.J. Šafarik University, Institute of Physics, Faculty of Science, Park Angelinum 9, 04154 Kosice, Slovakia*
**Corresponding author e-mail: artempogodin88@gmail.com*

Abstract. Herein we present the results of the study of ceramic materials made on the basis of Ag_8GeS_6 powders with different dispersion. The average grain size of microcrystalline powders is 10…20 μm, and that of nanocrystalline powders is ~140 and ~180 nm, respectively. The powdered materials were investigated using the XRD and SEM methods. The Ag_8GeS_6-based ceramic samples were obtained by annealing (1073 K) of pressed (400 MPa) discs. Investigations of the ceramics surface by using the SEM and EDS methods indicate the homogeneity of the chemical composition of the obtained ceramics. The electrical conductivity of the obtained ceramics was studied using impedance spectroscopy in a wide frequency ($1\cdot10^1$…$3\cdot10^5$ Hz) and temperature (293…383 K) ranges. For all these ceramics, an increase in electrical conductivity with increasing frequency is observed. Based on the obtained results, the values of ionic conductivity and activation energy of the corresponding Ag_8GeS_6 ceramic samples were determined.

Keywords: argyrodite, superionic conductor, ceramics, impedance spectroscopy, electrical conductivity.

https://doi.org/10.15407/spqeo26.03.270
PACS 66.30.Dn, 81.05.Je, 81.05.Mh, 82.45.Yz

Manuscript received 30.06.23; revised version received 24.07.23; accepted for publication 13.09.23; published online 20.09.23.

1. Introduction

Binary and more complex silver-containing compounds exhibit outstanding thermoelectric [1, 2], superionic [3, 4] or photovoltaic [5, 6] properties due to high electrical conductivity or light absorption. This is caused not only by the influence of the crystal structure of the compound as a whole, but also to the special arrangement of silver atoms. These compounds belong to different compositional and structural types. The most common are tetrahedrally coordinated compounds – derivatives of chalcopyrite (diamond-like) structure such as ternary $AgBiS_2$ or quaternary $AgCd_2GaS_4$ compounds and related to them kesterite/stannite Ag_2ZnSnS_4 phases [7]. The above-mentioned compounds are related to semiconductors and mostly exhibit photovoltaic or thermoelectric properties. In this aspect, compounds with an argyrodite structure are attractive. There exist two series of argyrodites – ternary ($x = 0$) and quaternary ($0 < x \leq 1$) with the general formula $M^{m+}_{(12-n-x)/m}N^{n+}X^{2-}_{6-x}Y^{-}_{x}$ (where M^{m+} – mostly single charged small cations Li^+, Cu^+, Ag^+; N^{n+} – multicharged cations Ga^{3+}, Si^{4+}, P^{5+}; X^{2-} – chalcogenide anions and Y^- – halide anions) [8–10]. Tetrahedrally coordinated (by chalcogens) multicharged cations form a rigid anionic sublattice. The resulting voids are statistically occupied by single charged cations, forming a highly disordered cationic sublattice. The coexistence of a rigid anionic framework and a mobile cationic sublattice leads to high conductivity in the solid-state [8–10]. Furthermore, argyrodites are classified as thermoelectric materials when electronic conductivity predominates [11–13] and as superionic materials when ionic conductivity predominates [14–16].

Ternary argyrodite Ag_8GeS_6 crystallize in two polymorphic forms: low temperature (LT) orthorhombic (space group (SG) $Pna2_1$, a = 15.1469 Å, b = 7.4694 Å, c = 10.5842 Å [17, 18]) and high temperature (HT) cubic (SG F–43m, a = 10.70 Å [19]) modifications. Band structure calculations indicate that LT-Ag_8GeS_6 belongs to direct gap compounds with band gap values of 1.46 eV [20]. As a result, promising photovoltaic applications of Ag_8GeS_6 in nanocrystalline ink form have been reported [21, 22]. The ionic conductivity of LT-Ag_8GeS_6 single crystals, grown by direct crystallization from melt, is quite low – $4.09\cdot10^{-5}$ S/cm [18]. This isn't typical for argyrodites and is associated with a significant ordering of the LT-Ag_8GeS_6 structure [18]. It is known that

for polycrystalline materials (ceramics) the ionic conductivity depends on grain orientation and grain-boundary properties (grain-size effect) [23, 24]. Inspired by this fact, we performed the investigation of ionic conductivity of LT-Ag_8GeS_6-based ceramic materials fabricated from different dispersion powders.

2. Experimental

2.1. Sample preparation

Polycrystalline Ag_8GeS_6 was prepared from stoichiometric amounts of high-purity elemental components Ag (99.995%), Ge (99.9999%) and S (99.999%). The ternary argyrodite was synthesized by a direct single-temperature method in evacuated to 0.13 Pa silica ampoules. The maximum synthesis temperature was 1280 K (48 h) [18]. This temperature is 50 K above the melting point of Ag_8GeS_6 [18], which ensured good melt homogenization and complete synthesis. As a result of the synthesis, a polycrystalline bulk sample weighing 20 g was obtained.

The synthesized Ag_8GeS_6 was ground in an agate mortar and sieved through sieves with appropriate pore sizes, which allowed us to select a powder fraction with a particle size within the range of 10 to 20 μm (~1/3 of the mass). To obtain powders with smaller particle sizes, 2/3 of the synthesized material (~13 g) was separated into two parts and additionally ground in a PQ-N04 planetary ball mill (agate balls and mortar) for 30 and 60 min at 200 rpm.

The corresponding discs with a diameter of 10 mm and a thickness of 2-3 mm were fabricated from the obtained Ag_8GeS_6 powders by using the cold pressing technique. The pressing was carried out at the pressure close to 400 MPa, to a relative density of 91 ± 1% of the theoretical one, which was determined by hydrostatic weighing. The resulting discs were annealed in evacuated silica ampoules at a temperature of 1073 K for 36 h. The heating/cooling rate was 20 K/h. This procedure enabled to obtain high quality Ag_8GeS_6-based ceramics.

2.2. Methods

Investigations of Ag_8GeS_6 powders and ceramic samples were carried out using the following methods.

X-ray diffraction (powders): AXRD Benchtop (Proto Manufacturing Limited) – Bragg-Brentano θ/2θ parafocusing geometry, 10…90° 2θ angle scanning range with dynamic ROI (dynamic region of interest), Ni filtered CuK_α radiation, 1 s exposure. Phase analysis, diffraction peak broadening and crystallite size determination were performed using PDAnalysis software (supplied by Proto).

Scanning electron microscopy and energy-dispersive X-ray spectroscopy (powders and ceramics): SEM Vega Tescan 3 (secondary electron, backscattered-electron (SE, BSE) detectors, applied accelerating voltage was 30 kV, operation distance around 15 mm, equipped with an energy dispersive X-ray (EDS) detector (Oxford Instruments).

Electrochemical impedance spectroscopy (EIS) (ceramics): AT 2818 high-precision LCR meter – $1 \cdot 10^1 \ldots 3 \cdot 10^5$ Hz frequency range, 293…383 K temperature range, AC amplitude – 10 mV, gold contacts (chemical deposition method from solutions [25]). The analysis of the measurement results by using Nyquist plots [26, 27] was performed in ZView 3.5.

3. Results and discussion

3.1. X-ray powder diffraction

The phase analysis of the prepared powders was carried out by comparison of the experimental diffractograms with the known diffractogram of Ag_8GeS_6 [18]. No new diffraction peaks were observed in the diffractograms of the micro- and nanocrystalline Ag_8GeS_6 powders, indicating phase homogeneity and absence of degradation during the milling process. The obtained diffractograms, corresponding to Ag_8GeS_6 powders, with different degrees of dispersion, show a broadening of the diffraction peaks (Fig. 1) when passing from microcrystalline powders (agate mortar) to nanocrystalline powders (ball mill). To quantify the broadening of the diffraction peaks for nanocrystalline powders, the corresponding values of the full width at half maximum (FWHM) parameter were determined. The FWHM parameter was calculated for the most intense peak of the LT-Ag_8GeS_6 phase, which corresponds to the (022) plane (Fig. 1). The diffractogram of microcrystalline LT-Ag_8GeS_6 was used to determine the instrumental line broadening.

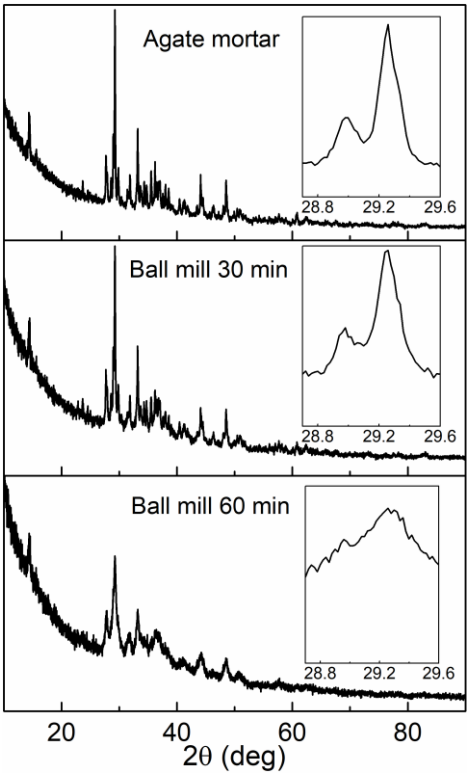

Fig. 1. Diffractograms of Ag_8GeS_6 powders obtained by mechanical grinding in an agate mortar and ball mill (for 30 and 60 min).

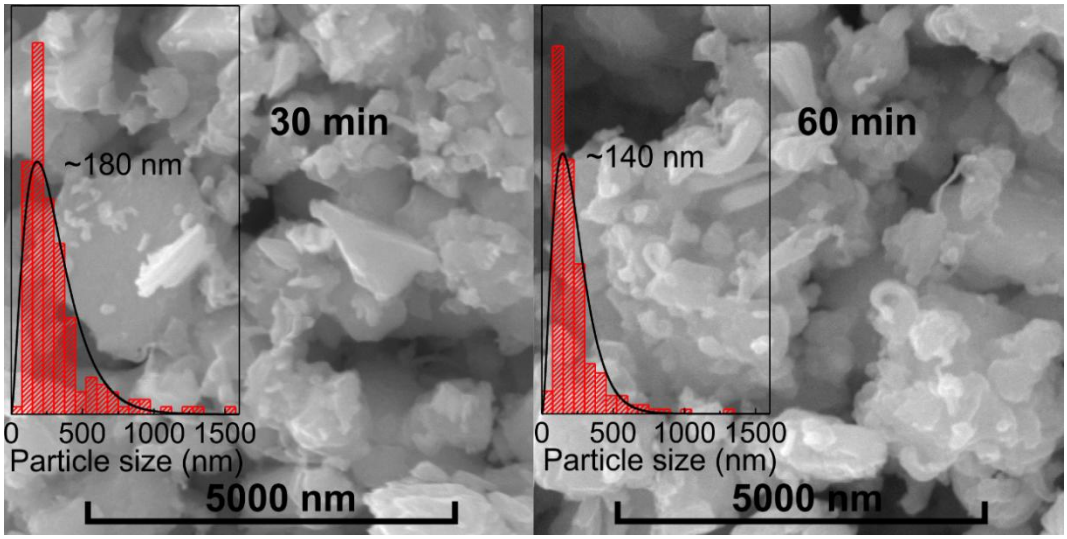

Fig. 2. SEM images of Ag_8GeS_6 powders obtained by grinding in a planetary ball mill. The inset shows the particle size distribution.

For the nanocrystalline powders obtained by grinding for 30 and 60 min, the FWHM values were found to be 0.1158° and 0.5181°, respectively. The determined FWHM values were used to estimate the size of crystallites according to Scherrer's equation [28]: $d = 0.89\lambda/\beta\cos\theta_\beta$. The applied Scherrer equation determines the particle size (d) as a function on the FWHM values of analyzed peak at the θ_β position and the X-ray wavelength (λ).

As the structure of LT-Ag_8GeS_6 belongs to the low symmetry class ($Pna2_1$), the corresponding diffractograms are complicated. This is reflected in the presence of a significant number of paired diffraction peaks, which complicates their analysis and makes it impossible to correctly determine the size of the crystallites. This is caused by the fact that the crystal size ($d_{60min} = 13 \pm 3$) was only determined for the powder ground for 60 min.

3.2. Microstructure

The SEM images of Ag_8GeS_6 powders obtained by grinding in a planetary ball mill (Fig. 2) revealed the presence of different sizes particles. It is also evident that the particles are highly aggregated, *i.e.*, they consist of smaller crystallites (Fig. 2). This is further confirmed by the XRD method, as the significant broadening of the diffraction peaks (Fig. 1) indicates the presence of nanoscale crystallites, which are aggregated into a larger particle. It was found that the average particle size obtained by grinding for 30 min is ~ 180 nm, while grinding for 60 min leads to a decrease in the average particle size to a value of ~ 140 nm (insets to Fig. 2). The tendency for the average particle size to decrease with increasing grinding time is accompanied by a narrowing of their distribution range, indicating the presence of a greater number of powder particles with similar size (insets to Fig. 2).

Let us consider the microstructure of ceramics made from microcrystalline (10…20 μm) and nanocrystalline (180, 140 nm) Ag_8GeS_6 powders (Fig. 3). For simplicity, the ceramics made from microcrystalline powder (10…20 μm) were referred to as Sample 1, those made from powder obtained by grinding in a planetary ball mill for 30 min (180 nm) as Sample 2, and those made from powder obtained by grinding in a planetary ball mill for 60 min (140 nm) as Sample 3. It is noteworthy that the microstructure of the studied Ag_8GeS_6-based ceramics (Samples 1–3) does not show clear grain boundaries between crystallites (Fig. 3). For this reason, it is not possible to determine the average crystallite size of ceramics Sample 1, Sample 2 and Sample 3. Only blurred intercrystalline boundaries and microstructural defects, such as small-angle boundaries and micro-voids, can be observed (Fig. 3). The occurrence of small-angle boundaries, which are best observed for Sample 1 (Fig. 3a), is related to the different crystallographic orientation of the crystallites in the powder and the pressed disc. The sintering of differently oriented crystallites leads to the appearance of this type of boundaries.

It should be noted that the number of micro-voids increases in the row Sample 1 → Sample 2 → Sample 3. This is due to the fact that a finer powder, in our case ~140 nm, has a higher surface free energy as compared to that for ~180 nm powder and 10…20 μm. As a result, recrystallization of a finer powder is much more efficient, which causes formation of more voluminous and concentrated micro-void areas (Fig. 3).

No less important is the homogeneous chemical composition of Ag_8GeS_6-based ceramics, as it is indicated by the uniform distribution of chemical elements on EDS maps (Fig. 4). It is noteworthy that

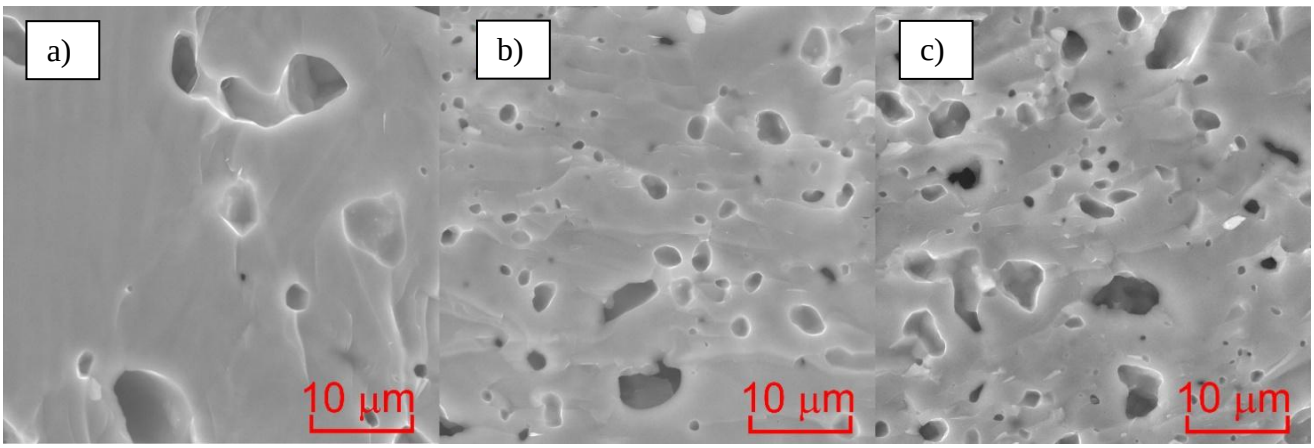

Fig. 3. SEM images of ceramics prepared by pressing and subsequent annealing of 10…20 μm (a), 180 nm (b) and 140 nm (c) Ag_8GeS_6 powders.

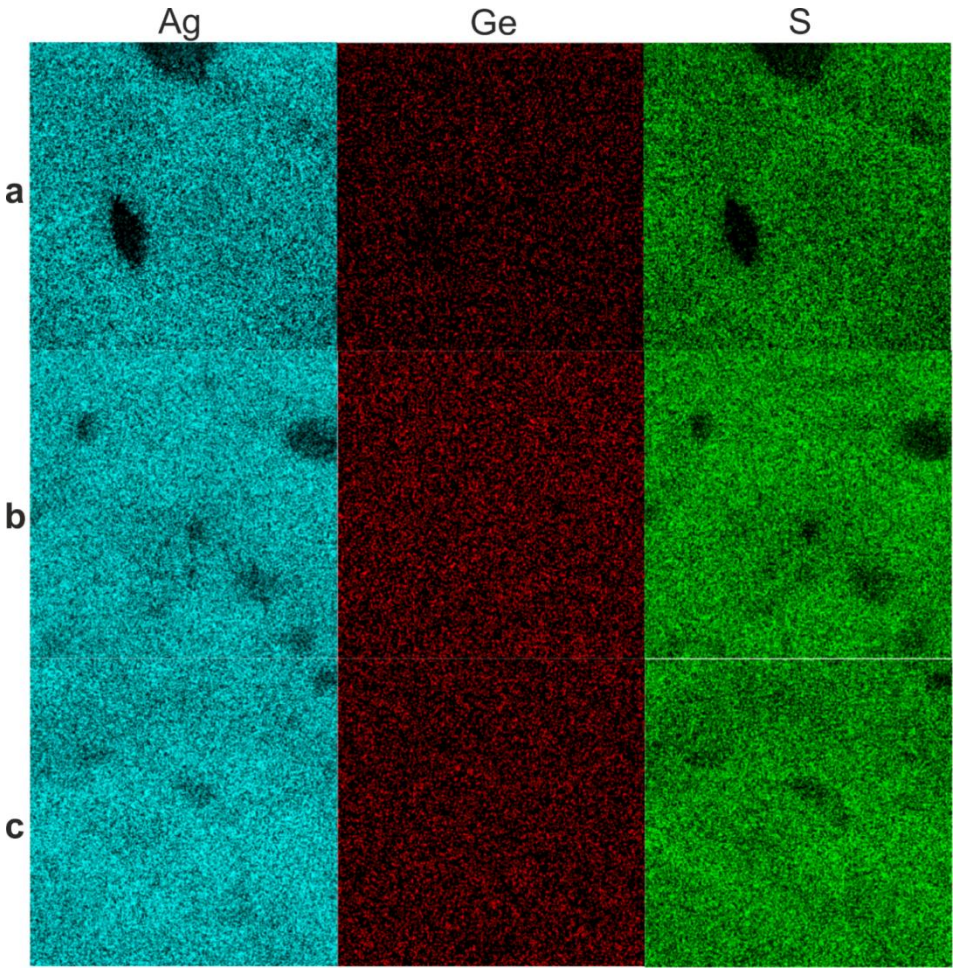

Fig. 4. EDS elemental distribution maps for Ag_8GeS_6-based ceramics: Sample 1 (a), Sample 2 (b) and Sample 3 (c).

darker areas can be observed on the EDS maps of Samples 1 to 3, which is especially noticeable on the Ag and S maps, *i.e.*, areas with a lower concentration of chemical elements, but these areas are located in the region of micro-voids (Fig. 4).

Considering the above results, it can be concluded that recrystallization of both micro- and nanocrystalline Ag_8GeS_6 powders does not lead to a significant deviation in the chemical composition of the corresponding ceramic materials.

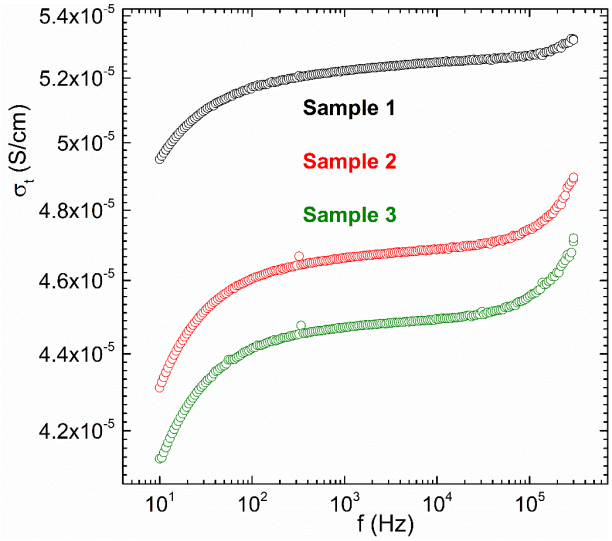

Fig. 5. Frequency dependence of the total electrical conductivity for ceramic materials made on the basis of Ag_8GeS_6.

3.3. Electrical conductivity

It has been ascertained that, for all Ag_8GeS_6-based ceramic materials (Fig. 5), the increase in frequency leads to a small increase in the total electrical conductivity, *i.e.* of the same order. This indicates a relatively low value of the ionic component of the electrical conductivity. This frequency behavior of the total electrical conductivity of Ag_8GeS_6-based ceramics (Fig. 5) is similar to that observed for single crystalline Ag_8GeS_6 [18].

To determine the ionic conductivity values of Samples 1–3 ceramics, the frequency dependence of the total electrical conductivity was analyzed using electrochemical equivalent circuits (EEC) in Nyquist plots (Fig. 6a). The analysis took into account the parasitic inductance of the cell, which is ~ 10^{-8} H.

Two semicircles are observed in the Nyquist plots (Fig. 6a) for all the Ag_8GeS_6-based ceramic materials (Samples 1–3) in the investigated temperature range. The low frequency semicircles in the Nyquist plots are responsible for the capacitance of double diffusion layer, which is marked as C_{dl} in EEC, while the appearance of high frequency semicircles is associated with inter-crystalline boundaries and defect boundaries (Fig. 3), which occur during recrystallization of micro- and nanocrystalline powders. In EEC, these semicircles are described by the resistance R_{gbi} with the parallel capacitance C_{gbi}. The resistance responsible for the electronic part of the electrical conductivity R_e affects the representation of both semicircles in Nyquist plots. EEC shown in Fig. 6a describes the frequency behavior of the total electrical conductivity over the entire temperature range studied. Thus, the value of the ionic component of the electrical conductivity can be set as $1/R_{gbi}$, and the electronic component as $1/R_e$.

Due to the rather low values of the electronic component of the electrical conductivity, it was not possible to determine it with sufficient accuracy, so we will focus on the consideration of the ionic conductivity only.

As a result of the analysis, it was found that the temperature dependence of the ionic component of the electrical conductivity for Samples 1–3 is linear (Fig. 6b), which indicates its thermoactivation character. As a result, the activation energies of the ionic component of the electrical conductivity were determined for all ceramic materials by using the Arrhenius equation.

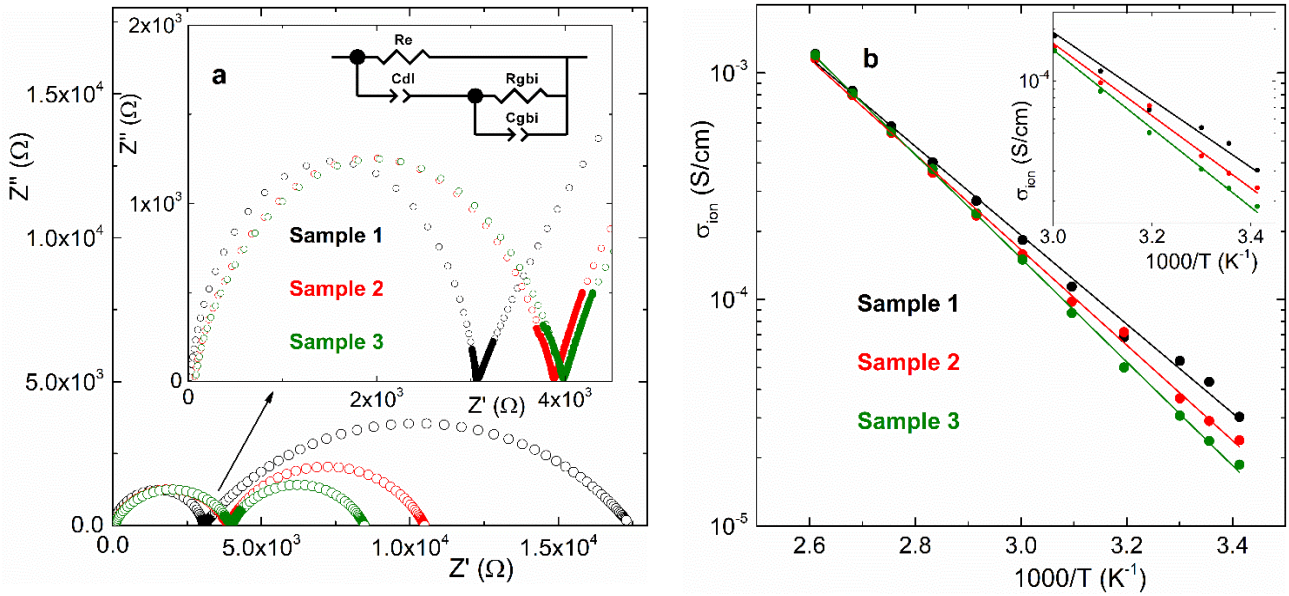

Fig. 6. Nyquist plots and EEC for ceramics made on the basis of Ag_8GeS_6 (a) (experimental data correspond to filled rings and calculated data – to unfilled rings) at 298 K; temperature dependence of the ionic component of the electrical conductivity (b).

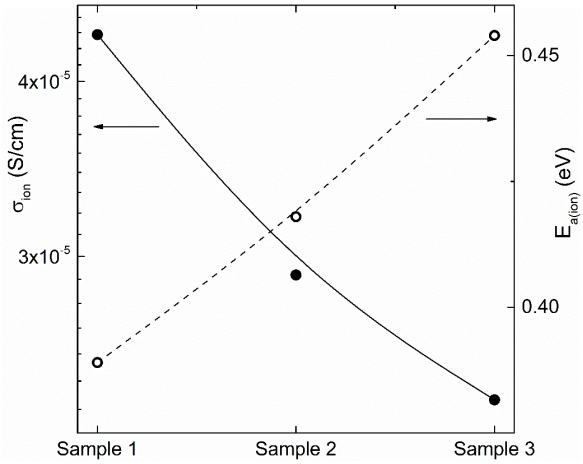

Fig. 7. Dependence of the ionic component of electrical conductivity and its activation energy for Samples 1–3.

It has been observed that the value of the ionic component of the electrical conductivity in the series Sample 1 → Sample 2 → Sample 3 is characterized by a monotonic decrease, while the value of the activation energy of the ionic conductivity increases monotonically. It is noteworthy that the increase in the ionic conductivity is insignificant, *i.e.*, within the same order of magnitude (Fig. 7). It should be noted that the value of the ionic component of the electrical conductivity for ceramic materials Sample 1–3 is commensurate with the corresponding one determined for the single crystalline Ag_8GeS_6 ($4.09 \cdot 10^{-5}$ S/cm) [18]. Moreover, the activation energy value for the Ag_8GeS_6 single crystal, which is 0.37 eV [18], is lower than for ceramics of the corresponding composition. This behavior may be related to an increase in the number of microdefects (Fig. 3) formed during recrystallization of micro- and nanocrystalline powders.

4. Conclusions

The synthesized polycrystalline Ag_8GeS_6 alloy was used to obtain powders with different degrees of dispersion. The microcrystalline powder was obtained using mechanical grinding in an agate mortar followed by sieving to obtain a fraction with a grain size of 10 to 20 μm. The nanocrystalline powders were obtained by grinding in a planetary mill for 30 and 60 min. As a result, nanopowders with an average crystallite size of 180 nm (30 min) and 140 nm (60 min) were obtained. Diffractograms of nanocrystalline Ag_8GeS_6 powders show a broadening of the diffraction peaks, which indicates a presence of nanoscale particles.

Based on the obtained micro- and nanopowder of Ag_8GeS_6 by a cold pressing technique, with a following annealing, ceramic samples were prepared. Investigation of ceramics microstructure by using the SEM method has shown that during the recrystallization process the grain boundaries between crystallites are not clear. Analysis of the obtained ceramics by using the EDS method indicates chemical homogeneity of ceramics, which is confirmed by a uniform distribution of chemical elements on EDS maps.

Investigation of Ag_8GeS_6-based ceramic materials by using the EIS method has shown the increase in total electrical conductivity with the frequency increasing, which is typical for superionic materials. Analysis of the obtained frequency dependences was carried out by means of Nyquist plots and electrochemical equivalent circuits. The corresponding values of ionic part of conductivity have been determined. Using the temperature dependence of conductivity, the activation energies of the ionic component of the electrical conductivity were determined using the Arrhenius equation.

Acknowledgements

The work at P.J. Šafarik University was supported by the grant of the Slovak Research and Development Agency under the contract APVV-20-0324. The authors would also thank the Armed Forces of Ukraine for providing security to perform this work. This work has become possible only because resilience and courage of the Ukrainian Army.

References

1. Tang Y., Yu Y., Zhao N. *et al.* High-performance thermoelectric α-$Ag_9Ga_{1-x}Te_6$ compounds with ultralow lattice thermal conductivity originating from Ag_9Te_2 motifs. *Angew. Chem. Int. Ed.* 2022. **61**. P. e202208281. https://doi.org/10.1002/anie.202208281.
2. Chen J., Yuan H., Zhu Y.-K. *et al.* Ternary $Ag_2Se_{1-x}Te_x$: A near-room-temperature thermoelectric material with a potentially high figure of merit. *Inorg. Chem.* 2021. **60**, No 18. P. 14165–14173. https://doi.org/10.1021/acs.inorgchem.1c01563.
3. Marple M., Kaseman D.C., Kim S., Sen S. Superionic conduction of silver in homogeneous chalcogenide glasses. *J. Mater. Chem. A*. 2016. **4**, No 3. P. 861–868. http://doi.org/10.1039/C5TA07301D.
4. Correa H., Lara D. Peña, Vargas R.A. Silver-ion dynamics close to the superionic phase transition of γ−$RbAg_4I_5$ with segregated Ag^+. *Phys. B: Condens. Matter*. 2019. **554**. P. 154–157. https://doi.org/10.1016/j.physb.2018.11.017.
5. Larsen J.K., Donzel-Gargand O., Sopiha K.V. *et al.* Investigation of $AgGaSe_2$ as a wide gap solar cell absorber. *ACS Appl. Energy Mater.* 2021. **4**, No 2. P. 1805–1814. https://doi.org/10.1021/acsaem.0c02909.
6. Bae S.Y., Oh J.T., Park J.Y. *et al.* Improved eco-friendly photovoltaics based on stabilized $AgBiS_2$ nanocrystal inks. *Chem. Mater.* 2020. **32**, No 23. P. 10007–10014. https://doi.org/10.1021/acs.chemmater.0c03126.
7. Shay J.L., Wernick J.H. *Ternary Chalcopyrite Semiconductors: Growth, Electronic Properties, and Applications*. Pergamon Press, Oxford, New York, 1975.
8. Kuhs W.F., Nitsche R., Scheunemann K. The argyrodites – a new family of tetrahedrally close-packed

structures. *Mat. Res. Bull*. 1979. **14**. P. 241–248. https://doi.org/10.1016/0025-5408(79)90125-9.
9. Nilges T., Pfitzner A. A structural differentiation of quaternary copper argyrodites: Structure – property relations of high temperature ion conductors. *Z. Kristallogr*. 2005. **28**. P. 1220–294. https://doi.org/10.1524/zkri.220.2.281.59142.
10. Deiseroth H.-J., Maier J., Weichert K. *et al.* Li_7PS_6 and Li_6PS_5X (X: Cl, Br, I): Possible three-dimensional diffusion pathways for lithium ions and temperature dependence of the ionic conductivity by impedance measurements. *Z. Anorg. Allg. Chem.* 2011. **637**. P. 1287–1294. https://doi.org/10.1002/zaac.201100158.
11. Lin S., Li W., Pei Y. Thermally insulative thermoelectric argyrodites. *Mater. Today*. 2021. **48**. P. 198–213. https://doi.org/10.1016/j.mattod.2021.01.007.
12. Studenyak I.P., Pogodin A.I., Luchynets M.M. *et al.* Influence of heterovalent substitution on structural, electrical and thermoelectric properties of $Cu_{7-x}PS_{6-x}Br_x$ solid solutions. *J. Phys. Chem. Solids.* 2021. **150**. P. 109855. https://doi.org/10.1016/j.jpcs.2020.109855.
13. Yang C., Luo Y., Li X., Cui J. N-type thermoelectric Ag_8SnSe_6 with extremely low lattice thermal conductivity by replacing Ag with Cu. *RSC Adv.* 2021. **11**. P. 3732–3739. http://doi.org/10.1039/D0RA10454J.
14. Chen H.M., Maohua C., Adams S. Stability and ionic mobility in argyrodite-related lithium-ion solid electrolytes. *Phys. Chem. Chem. Phys.* 2015. **17**, No 25. P. 16494–16506. http://doi.org/10.1039/C5CP01841B.
15. Adeli P., Bazak J.D., Park K.H. *et al.* Boosting solid-state diffusivity and conductivity in lithium superionic argyrodites by halide substitution. *Angew. Chem. Int. Ed.* 2019. **58**. P. 8681–8686. https://doi.org/10.1002/anie.201814222.
16. Pogodin A.I., Studenyak I.P., Shender I.A. *et al.* Crystal structure, ion transport and optical properties of new high-conductivity $Ag_7(Si_{1-x}Ge_x)S_5I$ solid solutions. *J. Mater. Sci*. 2022. **57**. P. 6706–6722. https://doi.org/10.1007/s10853-022-07059-1.
17. Eulenberger G. Die Kristallstruktur der Tieftemperaturmodifikation von Ag_8GeS_6. *Monatsh. fur Chem.* 1977. **108**. P. 901–913. https://doi.org/10.1007/BF00898056.
18. Pogodin A.I., Filep M.J., Izai V.Yu., Kokhan O.P., Kúš P. Crystal growth and electrical conductivity of Ag_7PS_6 and Ag_8GeS_6 argyrodites. *J. Phys. Chem. Solids.* 2022. **168**. P. 110828. https://doi.org/10.1016/j.jpcs.2022.110828.
19. Abbasova V.A., Alverdiyev I.J., Rahimoglu E. *et al.* Phase relations in the Cu_8GeS_6–Ag_8GeS_6 system and some properties of solid solutions. *Azerbaijan Chemical Journal*. 2017. **2**. P. 25–29.
20. Bletskan D.I., Studenyak I.P., Vakulchak V.V., Lukach A.V. Electronic structure of Ag_8GeS_6. *SPQEO*. 2017. **20**, No 1. P. 19–25. https://doi.org/10.15407/spqeo20.01.019.
21. Li Z., Liu C., Zhang X. *et al.* An easily prepared Ag_8GeS_6 nanocrystal and its role on the performance enhancement of polymer solar cells. *Org. Electron*. 2017. **45**. P. 247–255. https://doi.org/10.1016/j.orgel.2017.03.029.
22. He Q., Qian T., Zai J. *et al.* Efficient Ag_8GeS_6 counter electrode prepared from nanocrystal ink for dye-sensitized solar cells. *J. Mater. Chem. A.* 2015. **3**. P. 20359–20365. http://doi.org/10.1039/C5TA05304H.
23. van Dijk T., Burggraaf A.J. Grain boundary effects on ionic conductivity in ceramic $Gd_xZr_{1-x}O_{2-(x/2)}$ solid solutions. *phys. status solidi (a).* 1981. **63**. P. 229–240. https://doi.org/10.1002/pssa.2210630131.
24. Özbilgin C.E., Kobayashi K., Tamura S. *et al.* Enhanced ionic conductivity of aluminum tungstate by crystallographic orientation in a strong magnetic field. *J. Am. Ceram. Soc*. 2021. **104**. P. 6364–6372. https://doi.org/10.1111/jace.18001.
25. Studenyak I.P., Pogodin A.I., Filep M.J. *et al.* Crystal structure and electrical properties of Ag_6PS_5I single crystal. *SPQEO*. 2021. **24**, No 1. P. 26–33. https://doi.org/10.15407/spqeo24.01.026.
26. Huggins R.A. Simple method to determine electronic and ionic components of the conductivity in mixed conductors a review. *Ionics.* 2002. **8**, No 3. P. 300–313. https://doi.org/10.1007/BF02376083.
27. Vadhva P., Hu J., Johnson M.J. *et al.* Electrochemical impedance spectroscopy for all-solid-state batteries: theory, methods and future outlook. *ChemElectroChem.* 2021. **8**. P. 1930–1947. https://doi.org/10.1002/celc.202100108.
28. Muniz F.T.L., Miranda M.A.R., Morilla dos Santos C., Sasaki J.M. The Scherrer equation and the dynamical theory of X-ray diffraction. *Acta Crystallogr. A*. 2016. **72**. P. 385–390. https://doi.org/10.1107/S205327331600365X.

Authors and CV

Artem I. Pogodin, defended his PhD thesis in Inorganic Chemistry in 2016. Senior Researcher at the Uzhhorod National University. Authored over 100 scientific articles and 100 patents. The area of his scientific interests includes solid state chemistry, crystal growth and materials science.
https://orcid.org/0000-0002-2430-3220

Mykhailo J. Filep, defended his PhD thesis in Inorganic Chemistry in 2015. Senior Researcher at the Uzhhorod National University. Authored over 100 articles and 50 patents. The area of his scientific interests includes solid state chemistry and materials science. E-mail: mfilep23@gmail.com,
http://orcid.org/0000-0001-7017-5437

Serhii Vorobiov, defended his PhD thesis in Physics and Mathematics at the Sumy State University, Ukraine in 2015. Post-doctoral Researcher at the Institute of Physics, Faculty of Science, Pavol Jozef Safarik University, Slovakia. Author of 46 publications indexed in the Scopus and Web of Science databases as well as 1 patent. The area of his scientific interests includes nanofabrication and thin film technology, magnetic and magneto-resistance properties of nano- and mesoscopic systems.
E-mail: serhii.vorobiov@upjs.sk,
https://orcid.org/0000-0002-5884-3292

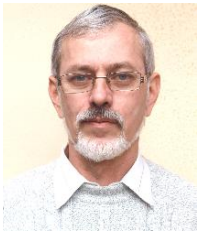

Oleksandr P. Kokhan, PhD, Associate professor of Inorganic Chemistry department, Uzhhorod National University. Authored over 80 articles and 95 patents. The area of his interests includes inorganic chemistry, solid state chemistry, crystal growth, materials science.
E-mail: aleksandr.kokh@gmail.com,
http://orcid.org/0000-0003-1534-6779

Tetyana O. Malakhovska, defended her PhD thesis in inorganic chemistry in 2010. Senior Researcher at the Uzhhorod National University. Authored 70 articles and 10 patents. The area of her scientific interests includes solid state chemistry and materials science.
E-mail: t.malakhovska@gmail.com,
https://orcid.org/0000-0001-7309-4894

Vladimir Komanicky, defended his PhD thesis in Chemistry in 2003 at the University of California. Leading Scientist in the Electrocatalysis and Nanotechnology group at the Institute of Physics of the P.J. Safarik University in Kosice. Author of 107 publications, 2 patents and two textbooks. The area of his scientific interests includes nanotechnology, electrocatalysis, semiconductor physics, magnetism and superconductivity.
E-mail: vladimir.komanicky@upjs.sk,
https://orcid.org/0000-0001-8649-1987

Vasyl V. Vakulchak, defended his PhD thesis in Physics and Mathematics in 2015. Senior Researcher of the Department of Applied Physics at the Uzhhorod National University. Authored over 80 publications and 1 patent. The area of his scientific interests includes *ab-initio* calculations of electronic structure and physical properties of semiconductors. E-mail: vasyl.vakulchak@uzhnu.edu.ua,
https://orcid.org/0000-0001-6037-8978

Authors' contributions

Pogodin A.I.: supervision, conceptualization, investigation, writing – original draft.
Filep M.J.: investigation, writing – original draft.
Vorobiov S.: investigation, visualization.
Komanicky V.: methodology, writing – review & editing.
Malakhovska T.O.: investigation, writing – original draft.
Kokhan O.P.: methodology, writing – review & editing.
Vakulchak V.V.: methodology, visualization.

Виготовлення та іонна провідність керамічних матеріалів на основі Ag_8GeS_6

А.І. Погодін, М.Й. Філеп, С. Воробйов, V. Komanicky, Т.О. Малаховська, О.П. Кохан, В.В. Вакульчак

Анотація. У даній роботі представлено результати дослідження керамічних матеріалів, виготовлених на основі порошків Ag_8GeS_6 з різною дисперсністю. Середній розмір зерна мікрокристалічного порошку становить 10…20 мкм, а нанокристалічних ~140 нм і ~180 нм. Порошкоподібні матеріали досліджено методами РФА та СЕМ. Керамічні зразки на основі Ag_8GeS_6 одержано відпалом (1073 K) спресованих (400 МПа) дисків. Дослідження поверхні керамік методами СЕМ та енергодисперсійної рентгенівської спектроскопії вказують на однорідність хімічного складу одержаних керамік. Електричну провідність одержаних керамік досліджено методом імпедансної спектроскопії у широкому частотному ($1\cdot10^1…3\cdot10^5$ Гц) та температурному (293…383 K) діапазонах. Для всіх керамік спостерігається зростання електричної провідності з підвищенням частоти. За одержаними результатами встановлено значення іонної провідності та енергії активації відповідних керамічних зразків Ag_8GeS_6.

Ключові слова: аргіродит, суперіонний провідник, кераміка, імпедансна спектроскопія, електрична провідність.